Characterisation of Cerebellar Efferents in Larval Zebrafish

A Thesis

submitted to

Indian Institute of Science Education and Research Pune in partial fulfilment of the requirements for the BS-MS Dual Degree Programme

by

Sudeepta Sarkar

Indian Institute of Science Education and Research Pune

Dr. Homi Bhabha Road,

Pashan, Pune 411008, INDIA.

Date: April, 2024

Under the guidance of

Dr Vatsala Thirumalai

Associate Professor

National Centre for Biological Sciences (NCBS-TIFR)

From May 2022 to Mar 2023

The thesis is dedicated to the butterfly that had set off the tornado.

Certificate

This is to certify that this dissertation entitled **Characterisation of Cerebellar Efferents in Larval Zebrafish** towards the partial fulfillment of the BS-MS dual degree programme at the Indian Institute of Science Education and Research, Pune represents study/work carried out by Sudeepta Sarkar at the National Centre for Biological Sciences (NCBS) under the supervision of Dr Vatsala Thirumalai, Associate Professor during the academic year 2023-24.

Dr Vatsala Thirumalai

Committee:

Dr Vatsala Thirumalai

Dr Raghav Rajan

Declaration

I hereby declare that the matter embodied in the report entitled **Characterisation of Cerebellar Efferents in Larval Zebrafish** are the results of the work carried out by me at the National Centre for Biological Sciences (NCBS), Bangalore, under the supervision of Dr Vatsala Thirumalai, and the same has not been submitted elsewhere for any other degree. Wherever others contribute, every effort is made to indicate this clearly, with due reference to the literature and acknowledgement of collaborative research and discussions.

Sudeepta Sarkar

Roll Number : 20191130

Table of Contents

List of Tables

List of Figures

Abstract

The cerebellum is known to be the major centre for motor learning in vertebrates. It has a well-conserved circuit architecture, where a layer of inhibitory neurons, called Purkinje neurons, receives a copy of the executive signals from the higher motor areas and error feedback from lower neurons, computes the 'error' and tunes the motor execution. Interestingly, not much is known about how cerebellar output executes motor error correction. In mammals, the output from the cerebellum is carried by the axons of the deep cerebellar nuclear cells (DCNs), which project to diverse brain regions, including the motor thalamus and the reticular formation. In this work, we have looked at the circuitry encoding cerebellar efferent signals using larval zebrafish as our model. In fish, Purkinje neurons project onto a group of glutamatergic neurons called the Eurydendroid cells (ECs), which are thought to be the equivalent of the mammalian DCNs. ECs have been shown to also project widely within the brain of the fish and thus are likely to play a critical role in conveying motor error correction information to their targets. However, not much is known about the inherent activity patterns of these neurons. We performed spontaneous in-vivo loose patch recordings from ECs of paralyzed zebrafish larvae. We describe two distinct populations of ECs in terms of their electrophysiological activity i.e. chatty (consistent/high spiking) and stuttering(irregularly spiking/low spiking). With pharmacological treatments, we also show that these neurons are inherently spiking. We also tried to look at the spatial distribution of the two kinds of ECs as a population. Hence, we performed two-photon calcium imaging and tried to classify the neurons based on their calcium activity. With further experiments, we hope to dissect the mechanisms underlying the distinct activity patterns of the two populations and what their roles might be in terms of cerebellar function. Thereafter, we hope to answer more general questions about the fundamental nature of the error correction implemented by the cerebellum.

Acknowledgement

Firstly, I want to express my sincere gratitude to my guide, Dr Vatsala Thirumalai, for helping me make sense of my own thoughts and for inspiring me with her vision and cultivating new ideas. I am grateful to Meha Jadhav, Shivangi Verma and Anzal KS for being the pillars of support in everything that I have done during my thesis work. I would also like to thank Dr Sriram Narayanan for teaching me two-photon microscopy and getting me used to working with optical devices. I also thank Mr Jagadeesh P.T. for taking care of the fish that I did my experiments on. Lastly, I would like to thank all the lab members of Dr Vatsala Thirumalai, Dr Upinder Singh Bhalla, Dr Anjana Badrinarayanan and Dr Deepa Agashe labs for their constant help and support.

I am immensely thankful to my parents for being the voice of reason in every decision during my journey and caring for me when I did not. None of this would have been possible without my friends being there at every step, especially Kritika, Shivang, Shivani, Shruti, Sahil and Sumit. I cannot thank them enough for their infinite patience and for never giving up on me.

Finally, I would like to thank the facilities at NCBS for their constant support. I thank IISER Pune and NCBS Bangalore for giving me the opportunity to work on this project and the INSPIRE-SHE (KVPY) scholarship for their funding.

Contributions

Contributor name	Contributor role
Sudeepta Sarkar and Dr Vatsala Thirumalai	Conceptualization Ideas
Sudeepta Sarkar and Dr Vatsala Thirumalai	Methodology
Sudeepta Sarkar	Software
Dr Vatsala Thirumalai	Validation
Sudeepta Sarkar and Dr Vatsala Thirumalai	Formal analysis
Sudeepta Sarkar	Investigation
Dr Vatsala Thirumalai	Resources
Sudeepta Sarkar	Data Curation
Sudeepta Sarkar	Writing - original draft preparation
Dr Vatsala Thirumalai	Writing - review and editing
Sudeepta Sarkar	Visualization
Dr Vatsala Thirumalai	Supervision
Dr Vatsala Thirumalai	Project administration
Dr Vatsala Thirumalai	Funding acquisition

Introduction

Creating motion is one of the most primal functions that the brain performs, so much so that it has been stated sometimes that the brain exists just to generate active movements. Like every biological system, the brain is also noisy and often commits errors. Unlike procedural errors that are committed while learning new skills, which over time get diminished, there are more frequent errors that occur when the intended and the executed actions do not match when performing, say, a nuanced motor task. These need to be corrected 'online' as and when the actions are getting done.

The cerebellum is known to act as the major centre for the correction of such motor errors, especially in the case of voluntary movements (Diener et al., 1992; Proville et al., 2014; Stein & Glickstein, 1992). It is understood that it works at multiple timescales so as to iteratively minimize the discrepancy between what is intended and what is executed (Barri et al., 2022; Boven & Cerminara, 2023; Braitenberg, 1967). Along with motor functions, recent findings also suggest the involvement of the cerebellum in the processing of emotional states and other higher cognitive functions(Schmahmann, 2019; Sokolov et al., 2017).

The cerebellar circuit has been studied over decades, and we have a fair insight into the possible mechanisms by which the cerebellar processing neurons might compute the errors. However, very little is known about the neurons that feed the corrected signals back into the major motor executive circuits. These neurons are downstream to the cerebellar cortical neurons, i.e. the computational units of the cerebellum, and have extensive projections to multiple regions in the entire brain (Baumel et al., 2009; Heap et al., 2013). In this study, we have tried to unravel what exactly is encoded in these signals that emerge out of the cerebellum, i.e. the way cerebellar efferents 'represent' the corrected signal.

Internal models and execution errors

Throughout the living world, animals have evolved different kinds of motor behaviours, befitting their ecological niches. Parallely, they have evolved neural systems that can cater to their specific motion requirements. These motor systems can not only robustly induce multiple kinds of motor commands but also can rapidly tune the action based on recurrent feedback loops from the sensory and higher-processing systems. Motor commands from the brain can be both voluntary (like walking) and involuntary (like breathing), and animals have architecturally laid out neural circuits to implement them. The general schema of these circuits has the higher motor centres (e.g. primary motor cortex in mammals, etc.) sending out efferent signals to spinal cord motor circuits from where motor neurons send commands to the muscles and where the action is finally performed. One can hence see an action as a coordinated series of muscle contractions orchestrated by the brain and spinal cord circuits. These circuits are sensorimotor integrators that bring different contexts of the motion together to execute and fine-tune the attempted motion (Umeda et al., 2022). The way in which the sensory inputs modulate the motor output is also subtle, as the sensory modalities linked to an action can be varied. There are neural circuits to collate sensory information and 'transform' them to make sense of the input in the context of the implemented motion. In vertebrates, this 'making sense' is what is often done in the cortical or cortex-equivalent processing regions (e.g. cerebellar cortex, pre-frontal cortex, etc.), after which the information is sent back to the central motor execution circuits, often via the thalamic and mid-brain centres. What the brain makes is called an 'internal model' of the external world and actively tunes it so as to go about performing what it needs to (Ito, 2008a; Narayanan & Thirumalai, 2019). Understandably, the internal model is ever-changing and holds the ability to optimise the motion output in a predictive manner. Differences with respect to the expected execution, hence, is evidence that needs to be processed to update the internal model. This is where cerebellar learning comes into play as it forms internal models of the action by optimising the error between the expected (internal model) and the executed (sensory feedback that contains evidence).

One of the most acclaimed theories of cerebellar learning came from Marr, Albus and Ito, who formalised a theory of iterative regression to correct motor errors. The theory has several forms and explains neural computation in terms of a balance between conditional long-term potentiation and conditional long-term depression of the synapses in the cerebellar cortex. The concept of the 'internal model' was also formalised by Ito and different versions of their suggested ideas have been tested in the cerebellar circuitry. Their theories have shaped most of the current understanding of cortical cerebellar computation. Still, how the optimisation is returned to the central circuits during the iterations is not clear (Ito, 2008b; Ito et al., 1982; Kawato et al., 2021)

Functional organisation of the cerebellar error correction circuitry

Theoretically, to correct errors, a system needs to have two kinds of information. There needs to be an input that describes the intended state and one that signals the feedback. In the most general cerebellar circuit, the major computation is carried out by a group of neurons called Purkinje neurons. Their cell bodies are mostly found at the base of the cerebellar cortex, and they receive signals at their enormous dendritic arbours spread out in the cortical neuropil or the molecular layer. The layer ventral to the Purkinje Neuron layer consists of much smaller but much more numerous Granule cells. Granule cells receive glutamatergic inputs from the mossy fibres coming from all over the brain. These synapses are specialised, with inhibitory Golgi cells making simultaneous synaptic contacts with the Granule cells where the Mossy fibres synapse. These three-way cerebellar synapses are called 'glomeruli'. Granule cells have about four dendritic arms where they receive signals, and further, these neurons make glutamatergic projections onto the Purkinje Neurons as parallel fibres (Consalez et al., 2021). These cells are known to bring in a very dense representation of the contextual information of the motion state (Giovannucci et al., 2017).

The molecular layer's other important input comes from the inferior olivary nucleus present in the brainstem. The fibres from the Inferior Olive decussate and enter the contralateral cerebellar cortices. They have gained a special name, i.e. climbing fibres, due to their peculiar organisation in the Purkinje cell layer as they quite literally wrap

around the proximal dendrites of the Purkinje Neurons. The Climbing fibres are also glutamatergic, and their release results in huge calcium spikes in the Purkinje neurons. These have atypical spike shapes distinct from the ‘simple’ spikes that Purkinje neurons fire. These are called ‘complex’ spikes. It is believed that the climbing fibres bring in the error feedback from the sensory circuits during motion and serve as a teaching signal (Bouvier et al., 2018; Zang & De Schutter, 2019).

The processing happens in the Purkinje Cells that finally project onto the deep cerebellar nuclei. These groups of cells constitute the major output of the cerebellum and send patterned projections to several circuits all over the brain. In mammals, these are a set of three nuclei, namely, fastigial, interposed and dentate nuclei. They show marked rebound spiking and are known to be inherently active (Baumel et al., 2009).
The two streams of cerebellar inputs described above, although discussed mostly in the context of the mammalian cerebellum, are starkly conserved across the vertebrates. However, mammalian systems provide unique challenges in investigating the functioning of this circuitry. Firstly, *in vitro,* preparations mask the true circuit-engaged activity of these neurons. Secondly, neurons often require non-biological concentrations of ions in the artificial cerebrospinal fluid to keep them alive in slices, which might affect the biophysical properties of the neurons. Due to their conserved fundamental connectivity, animal models like zebrafish provide potent alternatives. Given that the circuit is largely conserved across the vertebrate kingdom, the underlying basis of the computation can be hoped to be conserved as well.

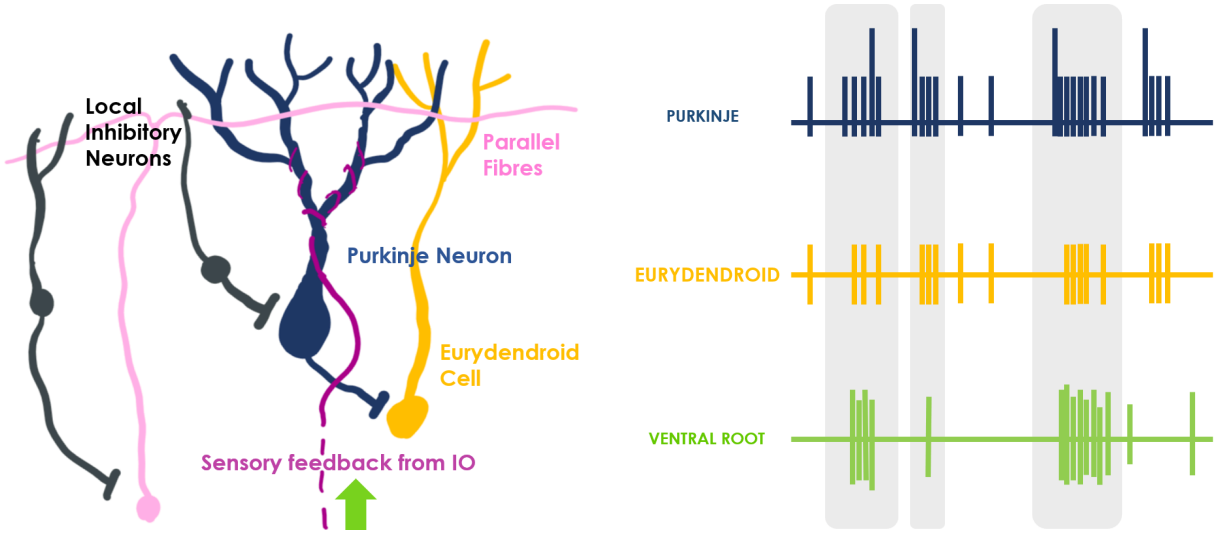

Figure I1: Schematic of the cerebellar circuitry in larval zebrafish

This figure summarizes the circuitry of the zebrafish cerebellum. Previous work (Najac et al., 2023; Sengupta & Thirumalai, 2015) and unpublished data from the lab suggest that the swim bouts of the fish (measured as fictive motor recordings from the ventral root) are coincident with bursts of activity in Purkinje Neurons and Eurydendroid cells.

Interestingly, when we look at the cerebellar efferents in models like zebrafish as well, much of the information about their organization and function is unknown. In contrast with the cell bodies being arranged in nuclei in the mammalian cerebellum, the fish cerebellar efferents are constituted by a layer of neurons called eurydendroid cells. These cells receive projections from Purkinje neurons and project to both ipsilateral and contralateral tectal and telencephalic circuits (Heap et al., 2013; Murakami & Morita, 1987). ECs have been reported to be predominantly glutamatergic exclusively. They also subtly differ in their excitatory inputs. The general consensus is that they receive glutamatergic inputs from parallel fibres in the molecular layer, and there are no reports yet of synapses from inferior olive neurons. DCNs, on the other hand, are known to receive inputs from mossy fibres and inferior olive collaterals. Although the major DCN projections to the cortex are glutamatergic, there are reports of GABAergic and Glycinergic efferents.

Recent studies have shown that the Eurydendroid cells fire concomitantly with swim bouts and show tuning in their firing activity upon motor learning (Harmon et al., 2020;

Najac et al., 2023). Distinct populations of these cells can be marked by markers like Calretinin and Olig2 (Bae et al., 2009; McFarland et al., 2008). However, the core microcircuitry of these neurons, or how their electrical activity is shaped by Purkinje neuron activity, is still unclear.

Overview of the thesis

We have employed approaches of *in-vivo* patch-clamp electrophysiology and functional imaging to tackle these questions at both cellular and population levels. We first identified sub-groups of neurons within the layer of ECs that have distinctly different spiking patterns. Using calcium imaging, we tried to map out the spatial distribution of these populations on the cerebellum. Finally, using pharmacology, we addressed how the microcircuitry of the inputs to the eurydendroid cells shapes its spiking pattern. We hope to answer whether the eurydendroid cells directly 'relay' the computation from the Purkinje neurons or whether there is a computationally significant synaptic transform that takes place between the cerebellar processing and the efferent neurons. If so, what is it that ECs encode and how? This will not only help us understand how the cerebellum talks to the motor systems at large but also might reveal fundamental principles behind the workings of cerebellum-like circuits that are found across the animal kingdom, not limited specifically to motor error correction.

Materials and Methods

Fish care, maintenance and animal ethics

The use of experimental animals (*Danio rerio*) was approved by the Institutional Animal Ethics Committee (IAEC) and the Institutional Biosafety Committee (IBSC). The adult fish were maintained in continuous water recirculation systems with controlled pH (7.2) and conductivity (1200 mS). The fish were reared in 14 hours of light and 10 hours of dark cycles, both the juveniles and the adults. The embryos were kept in petri dishes at 28℃ in water from the zebrafish facility for 4 days and then shifted to small tanks. The water also contains Methylene Blue (0.0005%) to prevent fungal growth. In case the fish needs to be screened, it is done after 4 days post fertilization so as to ensure. When raising fish, the larvae were maintained in small tanks without circulation for 10 days and then shifted to the main fish facility. The larvae and the adults were fed Zeigler diet of appropriate grain size. The juveniles and the adults in the fish facility were fed brine shrimp nauplii in one of the feedings during the day (Jadhav & Thirumalai, 2023).

Transgenic fish lines

The following genetic lines of zebrafish (*Danio rerio*) were used in this work (See Table M1) :

Table M1: List of fish genetic lines used

Sl No.	***Genotype***	***Expression***
1	*Tg*(*hspzGFFgDMC156A:GAL4,UAS:GFP*)	GFP in Eurydendroid cells
2	*Tg*(*hspzGFFgDMC156A:GAL4,UAS:GCaMP6s*, *nacre(-/-*)	GCaMP6s in Eurydendroid cells, larvae lack melanophores
3	Indian wild-type	N.A.

The *hspzGFFgDMC156A:Gal4* (*156A:Gal4* in short*)* is an enhancer-trap *Gal4* expressing line, made initially in the lab of Dr. Masahiko Hibi. This line expresses the yeast transcription factor Gal4 in cerebellar neurons, which have been identified as eurydendroid cells. Takeuchi et al. performed immunohistochemical staining to show that this population of neurons are glutamatergic and showed partial overlap with neurons expressing Olig2*,* which is a known Eurydendroid cell marker (Bae et al., 2009; Takeuchi et al., 2015). The *nacre* mutant contains a premature stop codon in the *microphthalmia*-related gene (*mitf*-related gene) 3A.1 in zebrafish. *microphthalmia* is a transcription factor involved in the development of eye and crest-pigment cells in mice. The mutation in the *mitf*-related gene in zebrafish causes a decrease in the number of melanophores, making it suitable for non-invasive *in-vivo* imaging experiments (Lister et al., 1999).

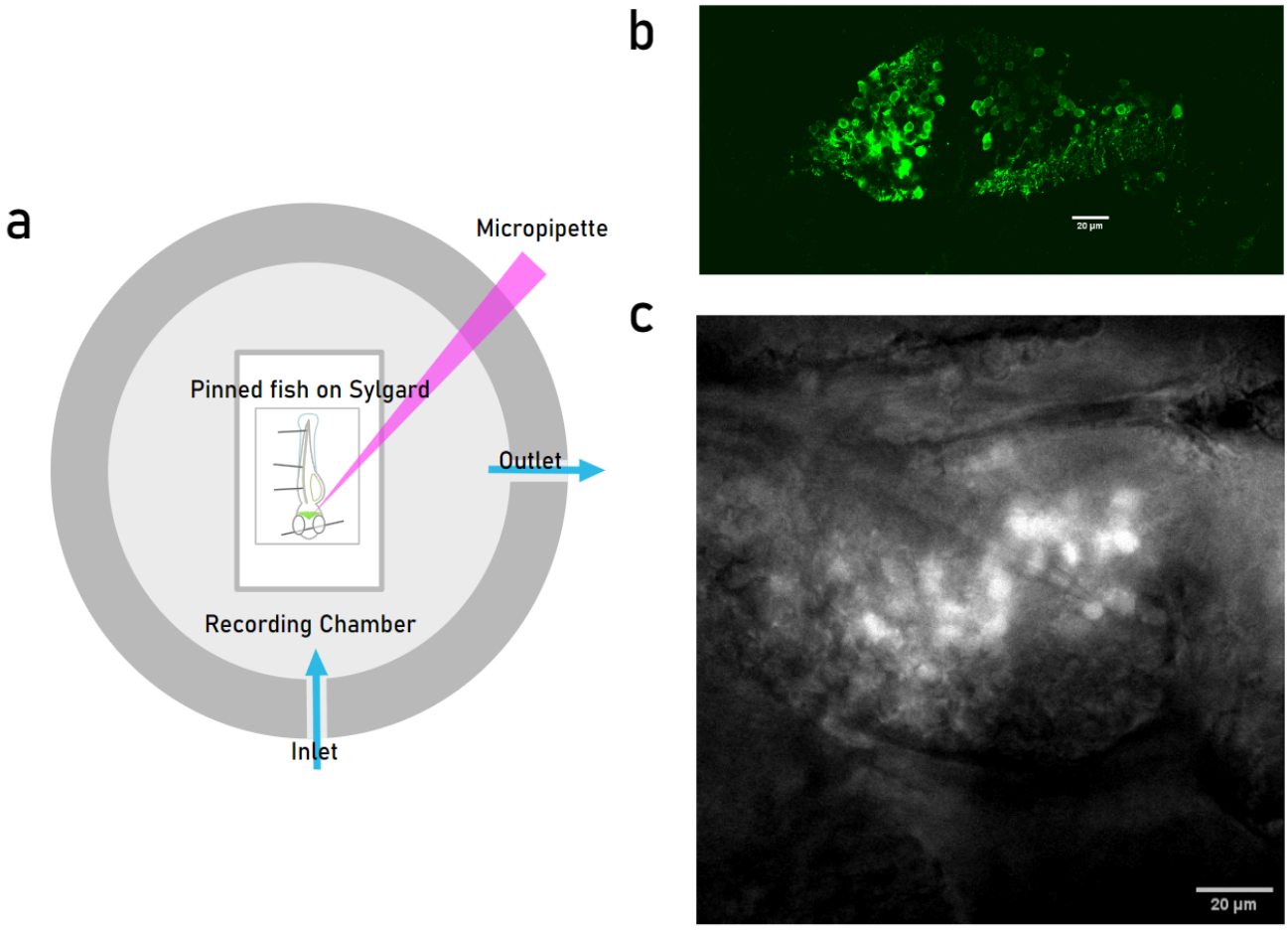

Figure M1: Schematic of the set-up for *in-vivo* electrophysiology

(a) The setup for electrophysiology
(b) Expression of 156A labelled ECs, anti-GFP IHC. Imaged By : Shivangi Verma
(c) Labelled EC under patch

Most of the experiments were performed with 6-8 days post-fertilisation (dpf) larval zebrafish. After collecting the embryos, they were kept in 90mm petri dishes until 3 dpf. They were screened for the desired expression under a table-top epifluorescence microscope (Olympus SZX16) with an oblique back illumination from a diffuse white light. The epifluorescence illumination was from an Olympus U-LH100HG Mercury lamp powered with an Olympus U-RFL-T power supply. The screened fish were maintained at a population of around 30 fish per tank (i.e. microtip boxes, without lid), filled with system water (pH ~7.8, conductivity ~1200 mS) and grown till the desired age, at around 27°C, in an incubator. To prevent unwanted fungal growth in the tanks, 0.03mM

Methylene Blue was added to the system water. For the in-vivo electroporation experiments, the fish were grown in 200 μM Phenylthiourea (PTU) diluted in this water from a 40X stock solution that is kept wrapped in aluminium foil at room temperature.

In-vivo electrophysiology

Dissection and Sample Preparation

All electrophysiological experiments are performed on 6-8 dpf larvae. The larvae expressing GFP in ECs are anaesthetised in 0.01% MS222 (Tricaine, Sigma) solution, prepared in fish-rearing water. Under anaesthesia, the fish is pinned on a Sylgard block in the recording chamber using cut pieces of Tungsten wire (dia: California Fine Wire Company) passing through the notochord at the mid-position, tail and above the air bladder. The last pin through the jaw is inserted such that the head of the fish is in a dorsal-up position. The tricaine solution is then replaced with external saline containing tubocurarine to paralyse the fish. The recording chamber is rinsed thrice with saline to ensure the removal of any traces of tricaine. The composition of external saline is given below (See Table 2):

Table M2: Composition of External Saline

Sl No.	Composition	Concentration
1	Sodium chloride	134 mM
2	Potassium chloride	2.9 mM
3	Calcium chloride	2.1 mM
4	Magnesium chloride	1.2 mM
5	D-glucose	10 mM
6	HEPES buffer	10 mM
7	α-tubocurarine	0.01 mM

The pH was adjusted to 7.78 - 7.8 using 3M NaOH and osmolarity to 295 - 300 mOsm. While immersed in external saline, the skin above the head of the fish is removed

carefully using a piece of Tungsten wire and fine forceps. Once the brain is exposed and the torn skin has been secured away from the brain, the preparation is taken for recording.

Electrophysiological Recordings

Recordings were done using filamented borosilicate glass micropipettes that were made by pulling borosilicate capillaries(1.5mm OD X 0.86mm ID, Harvard Apparatus) on a Flaming Brown P1000 micropipette puller (Sutter Instruments). With the external saline as the recording solution and a chlorided silver wire as the dipping electrode, the electrode assembly had a resistance of 8-10 MΩ in the bath. The recording solution was the external saline filtered through a 0.22 µm filter and contained sulphorhodamine (5 µg/mL) to visualise the flow under the microscope. The cells were identified under the FITC filter as they were expressing GFP. The filled pipette was attached to the pipette holder and manipulated close to the cell while applying positive pressure, which was released only at the surface of the cell. With slight negative pressure, a loose patch of 40-70 MΩ resistance was attained. The signal was acquired with a CV-7B headstage at 20 kHz with 200 amplifier gain on a Multiclamp 700B amplifier (Molecular Devices) and sent to the computer using a Digidata 1440A Digitizer (Molecular Devices). The recordings are digitally read and controlled with pCLAMP software suite (Molecular Devices). All the recordings have been performed in darkness unless mentioned otherwise.

Recordings with Pharmacological Treatments

For experiments that required pharmacological agents, the recordings were performed by superfusing the drugs in the bath. A flow of ~10 mL/min was maintained across the recording chamber by attaching an inlet tubing to a perfusion syringe and an outlet tubing to a vacuum manifold. After the flow control with external saline, the drug dissolved in external saline was allowed to superfuse completely by letting about 15 mL of the solution flow into the system. Multiple recordings of one minute each were performed within 5 - 7 minutes after the perfusion. The details of the drugs are given in the following table:

Table M3: Details of Pharmacological Drugs Used

Chemical Name	Make	Catalog No.	Concentration	Stock
NBQX	Tocris	373	20 µM	20 mM (DMSO)
Gabazine (SR95531)	Sigma Aldrich	S106	10 µM	10 mM (Water)

Analysis of Electrophysiology Data

Data were analysed with the Python package neo (https://neo.readthedocs.io/en/latest/), along with other standard packages. Spikes were detected from the original trace by scipy.signal package of Python and binarised into event plots for efficient handling. A rolling window of 1 second was rolled at 0.5 seconds to generate frequency plots for the time series.

In-vivo **Calcium Imaging**

Sample Preparation

Larvae were briefly immersed in 0.01% MS222 solution till they fell on their lateral side. They were immediately transferred to a solution of low-gelling agarose (2% w/v, Sigma-Aldrich) prepared in the system water. The fish was embedded in a drop of the agar and placed on the lid of a culture dish of 60mm diameter. It was made sure that the depth of the head of the fish was never deeper than about 1-2 mm from the upper surface of the droplet. For that, adding a drop of agar before placing the fish helps. After letting the droplet dry for around 15-20 minutes, it was immersed in system water before imaging.

2-Photon Calcium Imaging

Calcium activity was imaged from *Tg*(*156A:GAL4,UAS:GCaMP6s*), *nacre(-/-*) larvae at 6-8 dpf using a custom-built two-photon microscope. The laser power at the sample was kept below 20 mW. The microscope is controlled by ScanImage 3.8 (Pologruto et al.,

2003). An ROI was selected covering one lobe of the cerebellum, and frames were acquired at 7.81 Hz (3.2 µs pixel time) in an image of 256 X 128 pixels. For z-stack, the distance between each slice was kept at 1.5 µm so as to densely sample the entire layer of ECs. The acquisition and LASER power were optimised to accommodate the dynamic range of the cells in the field of view and the fluorescence rise and fall times of GCaMP6s.

Analysis of Calcium Imaging Data

Calcium trace extraction from time-series data using Suite2p

Fluorescence intensity traces were extracted from the imaging time series using the machine learning tool Suite2p. This was developed in the laboratory of Carsen Stringer and Marius Pachitariu and has been made open-source (Pachitariu et al., 2017; Stringer & Pachitariu, 2019). The vital parameters used for the extraction are as follows:

Table M4: Crucial parameters for Signal Extraction from Imaging Time-Series

Parameter	**Value**
tau	1.5
fs	7.8
anatomical_only	3
diameter	8

The module also provides a neuropil trace that is subtracted from the calcium trace frame-by-frame weighted by 0.7.

Metrics for Data Representation and Analysis

All the analyses were done using standard PYTHON libraries in a Jupyter notebook. The neuronal traces are represented as changes in fluorescence over baseline (ΔF/F). The baseline is considered to be the 10th percentile of all the data points in a trace. The ΔF/F trace is further smoothened by convolving it with a Gaussian filter with $\sigma = 3$.

Miscellaneous

In-vivo electroporation

To understand the convergence of Purkinje neuron inputs to ECs, we decided to perform neuronal tracing. The *Tg*(*156A:GAL4, UAS: GFP*) fish were treated with 200 µM PTU solution for depigmentation since 24 hpf. Once 6-8 dpf age is reached, they were embedded in 1% w/v low gelling agarose prepared in external saline. ECs were electroporated with Cholera-toxin Beta subunit tagged with Alexa Fluor 555(1 µg/µL, diluted in internal saline). The composition of the internal saline is as follows:

Table M5: Composition of External Saline

Sl No.	Composition	Concentration
1	Potassium Gluconate	115 mM
2	Potassium Chloride	15 mM
4	Magnesium Chloride	2 mM
5	EGTA	10 mM
6	HEPES Buffer	10 mM
7	Magnesium ATP	4 mM

The pH of the solution is set to 7.2, and the osmolarity is set between 290 - 295 mOsm (Jadhav & Thirumalai, 2023). Because the internal solution contains ATP, it was made into 1 mL aliquots and used only once after it was thawed. The electroporation set-up delivers pulses of -200 mV from the digitizer for a duration of 200ms after every ~4 seconds. The pulse is smoothened by passing it through a capacitor. After ensuring the cell fill by observing under an epifluorescence microscope, the fish is released from the agar and allowed to recover in Hank's solution (https://cshprotocols.cshlp.org/content/2006/1/pdb.rec548.full) for a day. They were planned to be imaged under a confocal microscope; however, the imaging and the recovery time could not be optimised.

Fluorescence in-situ Hybridisation

The 156A:*Gal4* is an enhancer-trap line made in the lab of Dr. Masahiko Hibi(Takeuchi et al., 2015). Earlier studies on ECs were mainly done in fish expressing fluorophores under the EC marker Olig2(Harmon et al., 2020; Najac et al., 2023). Calretinin is yet another marker for ECs, and it labels cells that are more ventral in the cerebellum. The Olig2 +ve and Calretinin +ve neurons are mutually exclusive. (Heap et al., 2013; McFarland et al., 2008).

We wished to validate the genotype of the neurons labelled under 156A using fluorescent *in-situ* hybridisation(FISH). From the ZFIN gene database, the cDNA sequences for *Olig2* (gene for Olig2) and *Calb2a* (gene for the expressed Calretinin, verified with Takeuchi et al. transcriptome data set) were taken. Primers were made for the UTRs, with overhangs for the restriction sites XhoI and SpeI(Table M5).

Table M5: Details of Primers used for FISH

Sl No.	**Primer Position**	**Primer Sequence**
1	*Olig2* Forward	5’-ccatggggaatagccttacaagtcaattctg-3’
2	*Olig2* Reverse	5’-actagtgattcccacaacacattgtttagtc-3’
3	*Calb2a* Forward	5’-ctcgagcgggattttcttgtggacagtatac-3’
4	*Calb2a* Reverse	5’-actagtcggttacagtattcaggcagc-3’

Total cellular RNA was extracted from the heads of 10 fish larvae at 10 dpf. Using reverse transcriptase (ABScript II-First Strand Synthesis Kit, ABClonal), cDNA was prepared for the mentioned genes.

It is planned to clone these gene sequences under T7 or T3 promoters and synthesize RNA probes labelled with Digoxigenin. These will then be used to label the cell populations. For visualisation, the signal will be amplified using Tyramide Signal Amplification (TSA) method.

UAS-eNpHR-EYFP Plasmid Construct

Purkinje neuron activity is heavily modulated by climbing fibre inputs (CF inputs) that cause huge calcium-driven depolarizations in the cell. Often, these CF inputs can lead to bursts and spontaneous shifts to the tonic state. We wanted to modulate the Purkinje neuron cellular state by silencing or activating the CFs. Additionally, fish also respond to visible light and show enhanced motor activity when exposed to blue light.

A red-shifted light-sensitive chloride channel (eNpHR) was planned to be expressed in the Inferior Olive neurons to enable light-mediated suppression of CF activity.

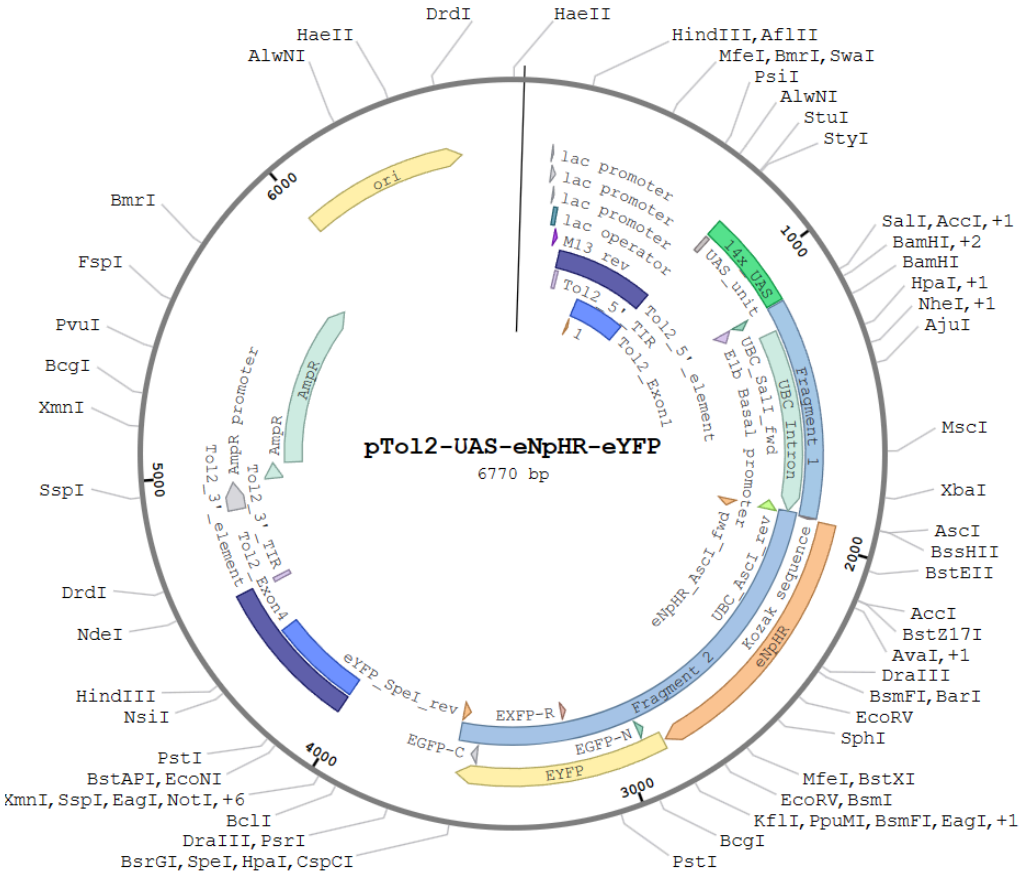

Figure M2 : Plasmid map of *pTol2-UAS-eNpHR-EYFP*

For this, the enhancer-trap line *Tg(hspGFFDMC28C:Gal4)* (expressed in the Inferior Olive) was planned to be microinjected with a plasmid containing the sequence

UAS-eNpHR-EYFP (Figure M2), flanked by Tol2 transposase binding sites. The sequence for 14X*UAS* repeats, and *UBC* intron was shifted from another plasmid (*UAS-CheRiff-tdTomato*) to *pAAV-eNpHR-EYFP* using restriction-digestion-based cloning. The construct was sequenced and made into plasmid stocks. The plasmids are to be microinjected in *Tg(hspGFFDMC28C:Gal4, UAS-CheRiff-tdTomato, nacre-/-)* embryos and screened for expression in the F1 progeny. Following that, the F1 offspring are to be incrossed to check for germline insertion.

Results

Eurydendroid cells have two electrophysiologically distinct sub-populations

We started by trying to understand the baseline spiking properties of the ECs; hence, we performed *in-vivo* loose patch recordings from these neurons. All experiments have been performed on larvae of age 6 - 8 days post fertilisation, expressing GFP in the ECs in a *Gal4*-enhancer trap line(156A)(Takeuchi et al., 2015). To ensure that the activity was truly spontaneous, lights and sound were minimised as much as possible during the recordings.

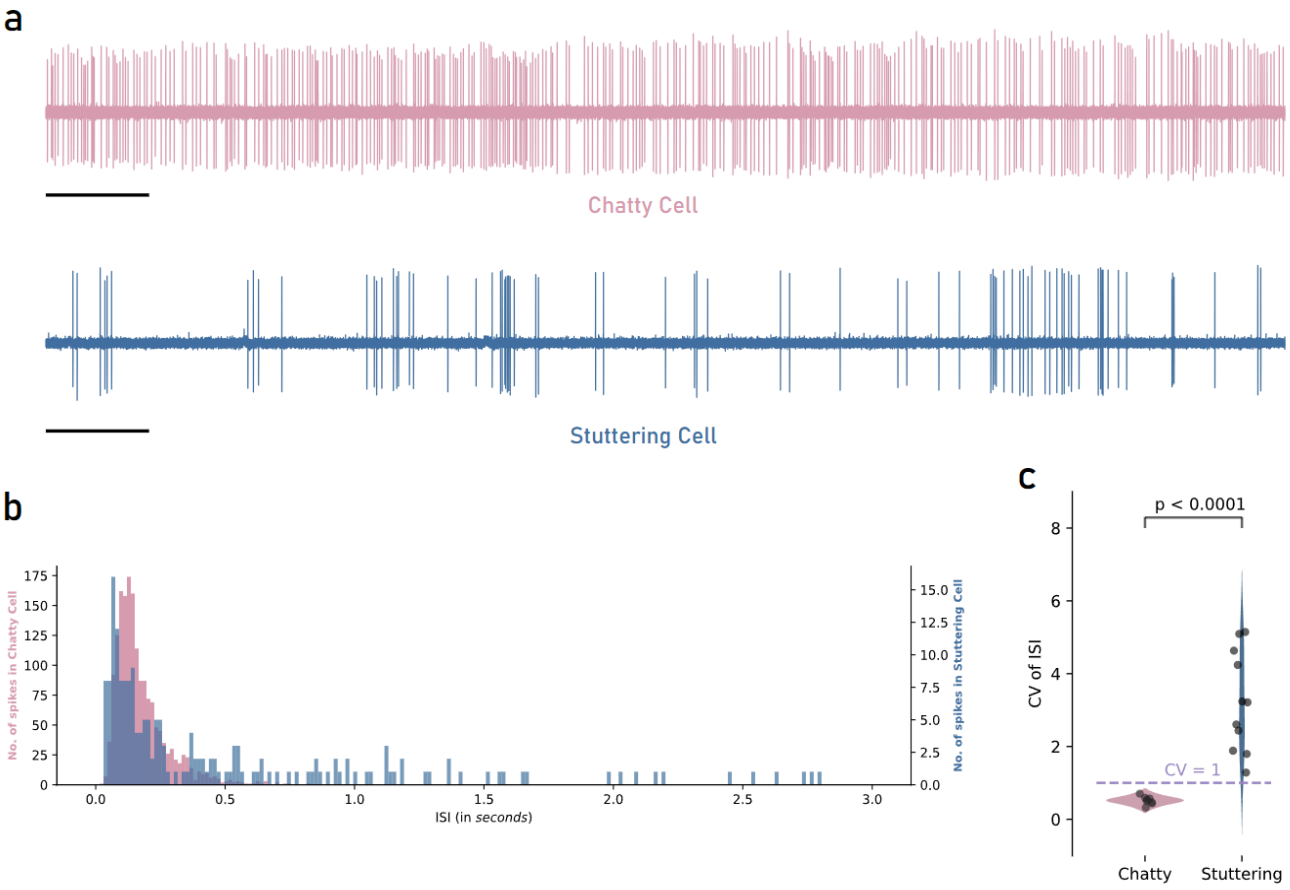

Figure R1: Baseline firing statistics of Eurydendroid Cells labelled under 156A Gal4 ET

(a) Representative traces of a chatty and a stuttering neuron. The colours red and blue represent chatty and stuttering throughout the report (*Scale Bar = 5 seconds*).
(b) The distribution of inter-spike intervals of the representative neurons. The left ordinate is for the chatty cell, and the right ordinate is for the stuttering cell. (The distribution is truncated at 3 seconds. It extends further to 14 seconds for the stuttering cell).
(c) The distributions of coefficients of variance of the chatty *(n = 8)* and stuttering cells *(n = 11)(Mann-Whitney Test p < 0.0001)*. CV = 1 of ISIs is taken as the decision boundary for classifying neurons as chatty or stuttering.

Similar to what has been described earlier, we find these neurons fire in two different ways. Some neurons show a near-periodic consistent spiking throughout the recordings, whereas some others have very inconsistent pauses ranging from tens of milliseconds to tens of seconds between subsequent spikes. The second kind often fires at a higher frequency for a short while before going silent for the next few seconds, resulting in small bursts of activity, along with jittered background spikes. We have called the former kind as ‘chatty cells’ and the latter as ‘stuttering cells’ (Figure 1a). The analysed baseline recordings are of five minutes each in darkness and silence. We have also done hour-long recordings (data not shown), but we have never seen any cell spontaneously switch its firing pattern from chatty to silent or vice-versa. Hence, we report that these are two electrophysiologically distinct populations and, unlike Purkinje neurons, do not show bistable activity states (Sengupta & Thirumalai, 2015).
Based on the earlier description, it was only natural to consider the coefficient of variance of their inter-spike intervals to be a reliable metric of classification. In Figure R1, the distributions of the CVs of ISIs are shown where we see that the CVs of chatty cells are strictly confined within 1, whereas the stuttering cells have CVs spread over a large range above 1. Hence, CV = 1 has been taken as the decision boundary between the two kinds of neurons.

Eurydendroid cell sub-populations are spatially organized in the cerebellum

While patching all across the cerebellum, we observed that the two kinds of cells are not spread randomly. The medial and ventral regions of the cerebellar lobes showed a

higher incidence of stuttering cells as compared to chatty cells. The latter is more prevalent towards the rostral and dorsal regions of the cerebellum.

To get a population-scale idea of the three-dimensional spatial distribution of these cell types, we performed *in-vivo* two-photon calcium imaging of the spontaneous activity of these neurons using the genetically encoded calcium sensor GCaMP6s (Figure R2).

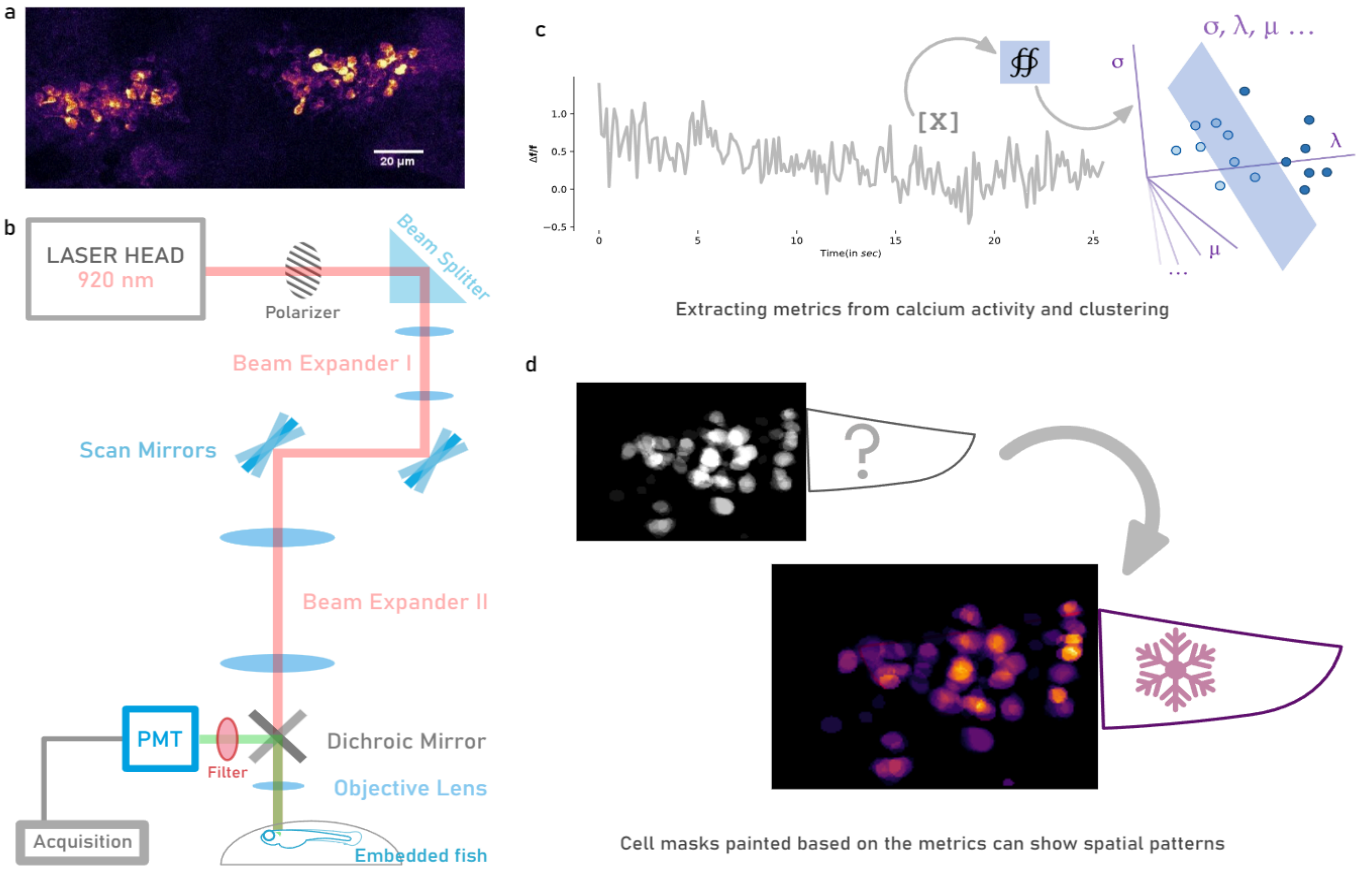

Figure R2: Spatial Organisation of Eurydendroid Cells

(a) Representative image showing 156A labelled ECs expressing GCaMP6s

(b) Schematic of the construction of the two-photon microscope used for imaging

(c) Schematic explaining extraction of meaningful metrics to understand the electrical activity of the cells and clustering them to find distinct physiological clusters based on the activity

(d) Extracted masks of cells coloured with metrics can reveal patterns of activity. In this example, the masks have been coloured based on the CV of the ROIs that were detected as cells.

The fluorescence response of GCaMP6s for a single action potential (a.k.a. The Green's function/ kernel for GCaMP6s) convolved with the spike times gives us the calcium activity regressor accompanying a cell's electrical activity. This is under the assumption that the significant calcium activity of a cell is solely dependent on its electrical activity, and one can infer one from the other. However, due to the limitations of the imaging paradigm in terms of temporal resolution, the fluorescence traces are severely downsampled. Hence, we have used statistical metrics to predict the electrophysiological identity of these neurons from their calcium traces.

We made 3D reconstructions of the Eurydendroid cells from the densely sampled two-photon imaging stacks using Fiji software. Using suite2p, an open-source machine learning-based tool (Pachitariu et al., 2017; Stringer & Pachitariu, 2019), we extracted the fluorescence traces from these cells using suitable parameters (discussed in Materials and Methods). The masks for the cell boundaries were also extracted. The cell masks were coloured based on the values of the metrics, and we can visualise how the cells are arranged in space. The analysis pipeline is ready, however, the imaging is yet to be standardised.

The example image (Figure R2d) shows the distribution of CVs of the calcium traces in the ECs. If we interpret using the idea of convolved ideal calcium activity from spike times, it is likely that the cells with higher CV will be stuttering neurons, and lower CVs will be chatty. In the reconstruction, we see that the cells in the medial and border regions have higher CVs than the rostral cells. Preliminarily, this seems to align with the observations we made during electrophysiology. A more in-depth analysis of the imaging paradigm and its shortcomings is continued in the discussion section.

Eurydendroid cells have inherently tonic firing activity

These cells, being the output neurons of the cerebellum, receive inputs from multiple excitatory and inhibitory cell types. The major inputs to these cells are the GABA-ergic inhibitory input from Purkinje neurons and the glutamatergic excitatory inputs from Granule cells (Harmon et al., 2020; Sengupta & Thirumalai, 2015). Inferior olive's

projection onto these neurons, although expected by homology to deep cerebellar nuclei of mammals, is not verified (Bouvier et al., 2018).

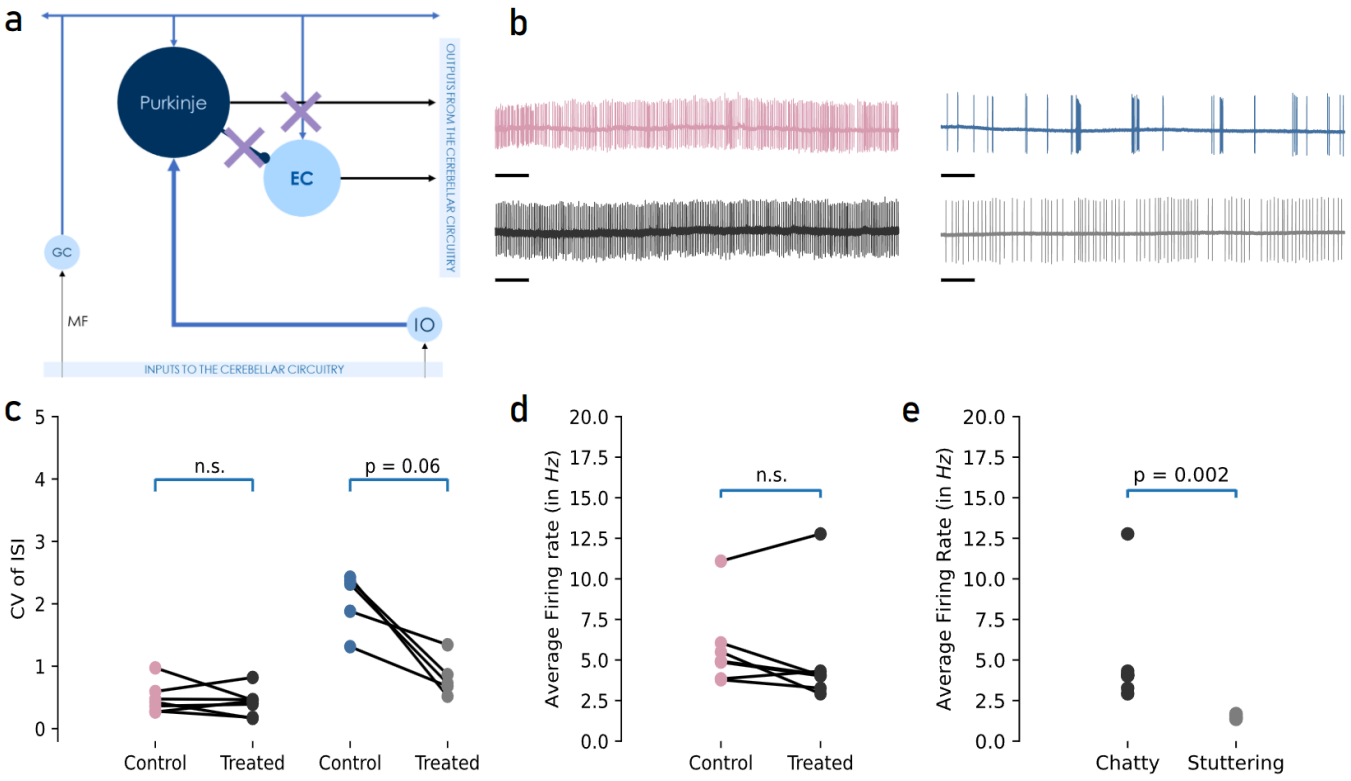

Figure R3: ECs with fast synapses blocked are inherently active

(a) Illustration describing the pharmacological experiment with NBQX and Gabazine. The AMPA-R-mediated inputs from granule cells and GABA-A mediated inputs from Purkinje neurons are blocked.

(b) Representative traces showing the change in the firing pattern of cells before (top) and after (bottom) the drug treatment (*Scale Bar = 5 sec*)

(c) The distributions of coefficients of variance of the chatty *(n = 7)* and stuttering cells *(n = 5)* before and after drug treatment.

(d) The firing rates of chatty neurons before and after drug treatment remain similar

(e) Average firing rates of chatty and stuttering ECs after the fast synapses are silenced (*Mann-Whitney Test, p = 0.002*)

For this, we tried to disconnect the cells from the circuit by blocking all the synaptic inputs. We added blockers for AMPA receptors (2,3-dioxo-6-nitro-7-sulfamoyl-benzo[f]quinoxaline or NBQX) and GABA-A receptors (SR-95531 or Gabazine) in the bath and recorded the neural activity pre and post-drug superfusion (Figure R3). Irrespective of the cell type (i.e. chatty or stuttering), as soon as the drug diffused in the bath, the cells showed multiple high-frequency spiking events (Figure R4b) and prolonged durations of no activity. In most recordings, the circuit-disengaged state appears to be a tonically firing state, irrespective of its initial category. However, we need more recordings to confirm the phenomenon.

The chatty neuron initial state and circuit disengaged state show very similar inter-spike interval distribution, even though they are fundamentally very different conditions (Figure R3d). Interestingly, in the disengaged state, we find that the frequencies of the chatty and stuttering neurons are significantly different, with the tonic frequencies of chatty cells being higher (1.51 ± 0.13 Hz for stuttering vs. 5.06 ± 3.18 Hz for chatty) (Figure R3e). The reason can be one of two: either the cells might be close but slightly different in their inherent properties, or there can be AMPA-independent excitatory currents that are still coming into the chatty neurons. Please refer to the discussion section for further analysis.

Inhibitory inputs to the Eurydendroid cells filter HFS events

Finally, we looked precisely at the connection of ECs with the principal computational units of the cerebellum, i.e. Purkinje neurons. We tried to block the inputs from the Purkinje cells to the ECs by superfusing only Gabazine in the bath and recording the firing activity before and after (Figure R4).

In the stuttering cells, the activity is discontinuous with multiple high-frequency bouts. These can also be categorised into two distinct kinds depending on the modulation of frequency within the bout; we called them ‘bursts’ and ‘HFS’ (for high-frequency spiking) events. Bursts are mostly short (~5 to 10 seconds), with the frequency peak averaging at around 6 Hz (5.8 ± 3.4 Hz). They sharply begin and end within a few seconds. HFS events happen on the order of tens of seconds where the frequency reaches about 34

Hz on average (34.3 ± 10.8 Hz). The fall of the frequency, in the case of HFS events, is also not sharp and is often accompanied by a lagging end that gradually reaches the baseline. HFS events are, however, not limited to stuttering cells; chatty cells can also show these long HFS events when stimulated with a brief exposure to blue light (Figure R4c).

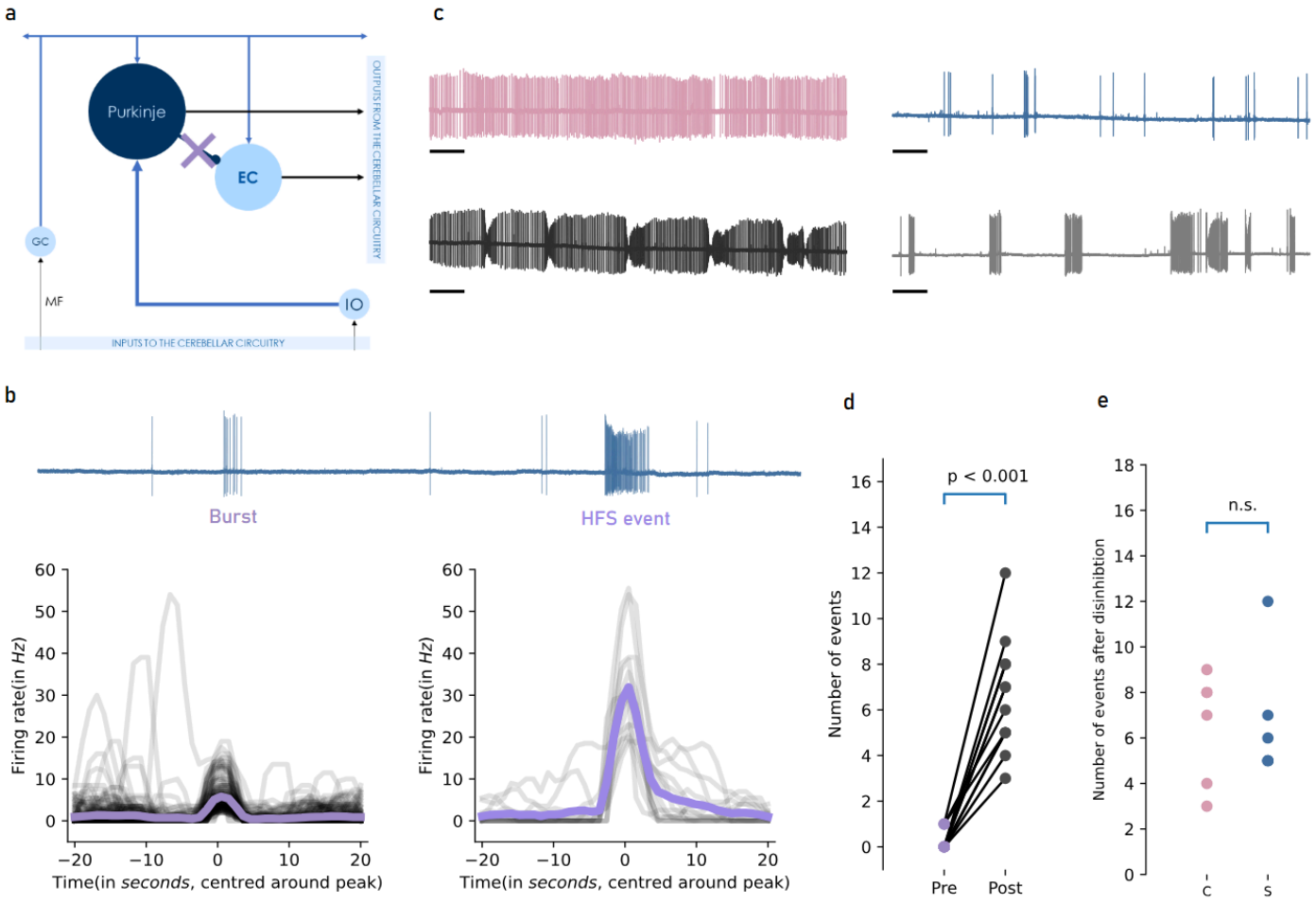

Figure R4: Disinhibited ECs show a higher number of high-frequency HFS events

(a) Illustration describing the pharmacological experiment with Gabazine

(b) Representative trace of a Stuttering neuron showing a baseline burst and HFS event. Overlay of spike frequencies during spontaneous HFS events and bursts

(c) Representative traces showing the change in the firing pattern of chatty (left) and stuttering (right) cells before (top) and after(bottom) the drug treatment (*Scale Bar = 5 sec*).

(d) The number of HFS events increases after the drug treatment (*p<0.001*, *Wilcoxon signed rank test*)

(e)The number of HFS events in chatty and stuttering neurons is similar in disinhibited ECs.(*p=0.87, Mann-Whitney Test*)

We see multiple high-frequency HFS events in both the chatty and the stuttering neurons (Figure R4b,d). In the initial few minutes during of the perfusion, the native activity of the cell could be seen accompanied by the HFS events coming over them periodically. Within a few minutes, often, there were multiple HFS events occurring aperiodically with long silent periods in between. The number of HFS events is comparable between chatty and stuttering disinhibited ECs (Figure R4e). However, the HFS events in chatty neurons seem to reach slightly lower frequencies at the peak as compared to stuttering neurons.

Discussion

We have characterised the spiking patterns and the underlying microcircuitry of ECs, the cerebellar output neurons in teleost fish. We performed *in-vivo loose* patch recordings and two-photon calcium imaging on larval zebrafish and tried to look at the spike statistics of these neurons. We identified two electrophysiologically distinct groups of neurons among eurydendroid cells: the chatty and the stuttering cells. We also tried to map the three-dimensional arrangement of these neurons in the cerebellum using two-photon calcium imaging.

To understand the micro-circuit influences, we recorded electrical activity from these neurons after the application of synaptic blockers. To look at the native circuit-disengaged state of ECs, we treated them with NBQX and Gabazine. In most cases, the cell attained a tonic firing state. Lastly, we blocked inhibitory inputs from Purkinje with Gabazine and observed a higher number of HFS events in ECs.

Sub-populations of Eurydendroid Cells

We reported that some ECs show tonic firing, whereas some fire at unpatterned intervals. We called them ‘chatty’ and ‘stuttering’, respectively. It is not surprising that the output neurons of the cerebellum have electrophysiological subpopulations, given its far and wide connections to multiple regions in the tectum and hindbrain. These neurons also show differences in terms of the molecular markers they express. Previous studies have shown that the molecular markers, Olig2 and Calretinin, label two mutually exclusive subpopulations of Eurydendroid cells (Bae et al., 2009; Heap et al., 2013; Hibi & Shimizu, 2012). Not only is their developmental landscape shaped by different cellular and molecular players, but also their anatomical arrangement is distinct, with Calretinin-positive neurons being ventral and Olig2-positive neurons being dorsal (McFarland et al., 2008). It will be interesting to look at the overlap between the

chatty/silent cells with Olig2/Calretinin-positive populations to understand their regionalisation and possible developmental trajectory. DCN neurons also show different electrically distinct subpopulations in terms of how they respond to stimulations such as hyperpolarizing current or harmaline, etc. Although, most of the DCN neurons seem to spike consistently, like the chatty cells (Baumel et al., 2009). Maybe, with more careful investigation, we will be able to draw parallels between the functional roles of the mammalian DCN and Eurydendroid cells.

Two-photon calcium imaging for neuronal identity

Genetically expressed calcium indicators (GECIs) have revolutionised the way we investigate the population activity of neurons and have been very successful in helping us understand the computational principles of neural circuits. The GECI that has been used in this work is GCaMP6s. This is a sixth-generation GECI that has a circularly permutated GFP molecule along with the calcium-binding region of Calmodulin (CaM). Upon binding to calcium, this region undergoes conformational changes and interacts with the M13 domain in the structure to sequester the GFP chromogenic centre away from water and; hence, it fluoresces with increased intensity (Chen et al., 2013; Remington, 2011). The ‘s’ in the name comes from ‘slow’, which refers to the kinetics of the GCaMP6 molecule. In our case, the slow GCaMP is a better option because of two primary reasons. The acquisition is a point scanning module, so the frame rates cannot get extremely high. As the GCaMP6s response falls over the order of a second, the Nyquist sampling rate can be achieved. With fast point-scanning systems, the signal-to-noise ratio might deteriorate if the sample is not bright enough, which is made sure with the higher brightness of GCaMP6s as compared to its contemporaries, i.e. GCaMP6f (‘f’ for fast) or GCaMP6m (‘m’ for medium)(Chen et al., 2013; Zhang et al., 2023).

For inferring the electrophysiological subtype, one needs to look at the electrical responses of the neuron. With the assumption that the calcium spikes in the cell are only due to calcium entry with depolarization mediated by action potentials, one might

attempt to infer spikes from the calcium traces. However, due to its slow kinetics, GCaMP6s is not very suitable. GCaMP6f can be a possible candidate, but it is not bright enough and too fast to optimally sample in our scope. One might use a light sheet imaging system with a widefield acquisition. Imaging GCaMP6s with one photon requires a 488nm laser as the excitation wavelength. But fish are sensitive to blue light and hence, the spontaneous activity would not be captured.

We are yet to finalise the metrics that can be used to classify the cell populations dependably. There are two possible approaches. One, we can perform simultaneous electrophysiology and calcium imaging from the same neuron. For this, we plan to simultaneously label the ECs with GCaMP6s and RFP. We will patch by looking at the RFP signal as it is bright and non-fluctuating, whereas GCaMP6s will help us image the calcium signal. The acquisition can be done at fast timescales with widefield microscopy, and the traces can be downsampled to make training datasets for machine learning algorithms to classify two-photon calcium traces (Varma et al., n.d.).

Alternatively, we can think about metrics that capture the variability/dispersion of cellular activity in terms of GCaMP fluorescence (e.g. coefficient of variance, the one used in Figure R2) and use those metrics to assign a neural identity in a ‘metric’-space and cluster them to see any kind of probable groups that might form. One can also try unsupervised time-series clustering on the calcium traces and see if any pattern emerges out of them. As in Figure R2d, we can replot the distributions of populations on the 3D masks of the cells and look at the spatial patterns, if any. Extending from the earlier discussion for looking at the overlap between the populations with distinct electrophysiological and molecular identities, one can perform fluorescence *in-situ* hybridisation after calcium imaging and visualize the two populations under a confocal or a lightsheet microscope.

External inputs drive the ECs to be chatty or stuttering

On disinhibiting the circuit using Gabazine, ECs fired multiple HFS events. Although the numbers might be an overestimate due to the increased firing of the granule cells as well, one can argue that the Purkinje neurons might be filtering the 'unnecessary' HFS events, only letting the required ones. In situations when the system is stimulated, say a visual stimulus, we see HFS events getting elicited in the Eurydendroid cells. The classical view of Purkinje neurons suggests that on coincident parallel fibre and climbing fibre inputs on the Purkinje dendrites, the synapses undergo long-term depression. Depressed synapses can delay the transmission through Purkinje, hence giving a window to the downstream ECs to fire, which we probably see as the hfs events there.

This might also suggest some deeper patterns in the arrangement of cerebellar circuits. If the climbing fibre inputs are indeed shaping the incidence of the HFS events in the eurydendroid cells, then the information from Inferior Olive is indirectly still reaching the eurydendroid cells, albeit through the Purkinje layer. When we compare to the mammalian DCNs and think about the possibility of inferior olive projections onto the ECs, it also seems likely that the 'format' of information that is analysed in ECs is fundamentally different from DCN. The inputs to DCN are mossy fibres and inferior olive. In ECs, we say the excitatory inputs are solely from parallel fibres; hence, the mossy fibre copy of the motor executive efferents from the higher brain centres is already filtered through the granule cell layer. Granule cells see a lot of local inhibitions mediated by cells like Golgi cells and also mix a lot of mossy fibre inputs given their cellular structure, suggesting that the synaptic transform at this layer is extremely non-trivial.

Looking at the circuit disengaged traces, we found that even in the absence of fast synaptic inputs, the neurons mostly fire tonically. This might mean that in the case of stuttering neurons, the inhibition is more than excitation, and hence, only a small amount of action potential gets ultimately fired in the check and balance, whereas the chatty neurons might be at total excitation-inhibition balance. This can be either due to

the numbers of convergence ratios of excitatory and inhibitory inputs, i.e. exactly how many Purkinje cells and parallel fibre synapses are synapsing onto the cells and with what synaptic strengths or there might be yet unreported positive currents that the cell is receiving. Notably, the tonic firing rate of initially chatty neurons was significantly higher than initially silent neurons. Cell-autonomous explanations can be differences in input resistance of the two populations due to differences in their geometry or ion channel expression landscapes. However, there might also be circuit influences that can provide constant excitatory currents. This is another way in which the climbing fibres might impact the activity of the Eurydendroid cells. Due to the huge synapses of climbing fibres at the Purkinje's primary dendrites, there is a lot of glutamate release in the ECM. One can also imagine that even after glial uptake, there might be 'spilt-over' glutamate present in the vicinity that is sufficient to set off NMDAR-mediated currents due to its high binding affinity to glutamate and expression not restricted to the post-synaptic density ((Kullmann & Asztely, 1998; Pankratov & Krishtal, 2003). From the transcriptome dataset of 156A labelled fish published by Takeuchi et al., it is evident that ECs do have higher numbers of NMDAR-related mRNAs. NMDAR currents are long and can be the putative source of long-drawn excitations that chatty cells require to attain their state. This is also hinted at by the arrangement of chatty and stuttering neurons in the calcium activity reconstructions, as we find the stuttering neurons are in the regions that are around the cerebellum and away from the major inferior olive tracts that project into the cerebellum.

References

1. Bae, Y.-K., Kani, S., Shimizu, T., Tanabe, K., Nojima, H., Kimura, Y., Higashijima, S., & Hibi, M. (2009). Anatomy of zebrafish cerebellum and screen for mutations affecting its development. *Developmental Biology*, *330*(2), 406–426. https://doi.org/10.1016/j.ydbio.2009.04.013
2. Barri, A., Wiechert, M. T., Jazayeri, M., & DiGregorio, D. A. (2022). Synaptic basis of a sub-second representation of time in a neural circuit model. *Nature Communications*, *13*(1), 7902. https://doi.org/10.1038/s41467-022-35395-y
3. Baumel, Y., Jacobson, G. A., & Cohen, D. (2009). Implications of functional anatomy on information processing in the deep cerebellar nuclei. *Frontiers in Cellular Neuroscience*, *3*. https://doi.org/10.3389/neuro.03.014.2009
4. Bouvier, G., Aljadeff, J., Clopath, C., Bimbard, C., Ranft, J., Blot, A., Nadal, J.-P., Brunel, N., Hakim, V., & Barbour, B. (2018). Cerebellar learning using perturbations. *eLife*, *7*, e31599. https://doi.org/10.7554/eLife.31599
5. Boven, E., & Cerminara, N. (2023). Cerebellar contributions across behavioural timescales: A review from the perspective of cerebro-cerebellar interactions. *Frontiers in Systems Neuroscience*, *17*. https://doi.org/10.3389/fnsys.2023.1211530
6. Braitenberg, V. (1967). Is the Cerebellar Cortex a Biological Clock in the Millisecond Range? In *Progress in Brain Research* (Vol. 25, pp. 334–346). Elsevier. https://doi.org/10.1016/S0079-6123(08)60971-1
7. Chen, T.-W., Wardill, T. J., Sun, Y., Pulver, S. R., Renninger, S. L., Baohan, A., Schreiter, E. R., Kerr, R. A., Orger, M. B., Jayaraman, V., Looger, L. L., Svoboda, K., & Kim, D. S. (2013). Ultrasensitive fluorescent proteins for imaging neuronal activity. *Nature*,

499(7458), 295–300. https://doi.org/10.1038/nature12354

8. Consalez, G. G., Goldowitz, D., Casoni, F., & Hawkes, R. (2021). Origins, Development, and Compartmentation of the Granule Cells of the Cerebellum. *Frontiers in Neural Circuits*, *14*. https://www.frontiersin.org/articles/10.3389/fncir.2020.611841
9. Diener, H.-C., Dichgans, J., Guschlbauer, B., Bacher, M., Rapp, H., & Klockgether, T. (1992). The coordination of posture and voluntary movement in patients with cerebellar dysfunction. *Movement Disorders*, *7*(1), 14–22. https://doi.org/10.1002/mds.870070104
10. Giovannucci, A., Badura, A., Deverett, B., Najafi, F., Pereira, T. D., Gao, Z., Ozden, I., Kloth, A. D., Pnevmatikakis, E., Paninski, L., De Zeeuw, C. I., Medina, J. F., & Wang, S. S.-H. (2017). Cerebellar granule cells acquire a widespread predictive feedback signal during motor learning. *Nature Neuroscience*, *20*(5), 727–734. https://doi.org/10.1038/nn.4531
11. Harmon, T. C., McLean, D. L., & Raman, I. M. (2020). Integration of Swimming-Related Synaptic Excitation and Inhibition by olig2+ Eurydendroid Neurons in Larval Zebrafish Cerebellum. *Journal of Neuroscience*, *40*(15), 3063–3074. https://doi.org/10.1523/JNEUROSCI.2322-19.2020
12. Heap, L. A., Goh, C. C., Kassahn, K. S., & Scott, E. K. (2013). Cerebellar Output in Zebrafish: An Analysis of Spatial Patterns and Topography in Eurydendroid Cell Projections. *Frontiers in Neural Circuits*, *7*, 53. https://doi.org/10.3389/fncir.2013.00053
13. Hibi, M., & Shimizu, T. (2012). Development of the cerebellum and cerebellar neural circuits. *Developmental Neurobiology*, *72*(3), 282–301. https://doi.org/10.1002/dneu.20875
14. Ito, M. (2008a). Control of mental activities by internal models in the cerebellum. *Nature Reviews Neuroscience*, *9*(4), 304–313. https://doi.org/10.1038/nrn2332
15. Ito, M. (2008b). Control of mental activities by internal models in the cerebellum. *Nature Reviews Neuroscience*, *9*(4), 304–313. https://doi.org/10.1038/nrn2332
16. Ito, M., Sakurai, M., & Tongroach, P. (1982). Climbing fibre induced depression of both mossy fibre responsiveness and glutamate sensitivity of cerebellar Purkinje cells. *The Journal of Physiology*, *324*(1), 113–134. https://doi.org/10.1113/jphysiol.1982.sp014103
17. Jadhav, M. P., & Thirumalai, V. (2023). *Ionic conductances driving tonic firing in Purkinje neurons of larval zebrafish* (p. 2023.11.29.569172). bioRxiv. https://doi.org/10.1101/2023.11.29.569172
18. Kawato, M., Ohmae, S., Hoang, H., & Sanger, T. (2021). 50 Years Since the Marr, Ito, and Albus Models of the Cerebellum. *Neuroscience*, *462*, 151–174.

https://doi.org/10.1016/j.neuroscience.2020.06.019

19. Kullmann, D. M., & Asztely, F. (1998). Extrasynaptic glutamate spillover in the hippocampus: Evidence and implications. *Trends in Neurosciences*, *21*(1), 8–14. https://doi.org/10.1016/S0166-2236(97)01150-8
20. Lister, J. A., Robertson, C. P., Lepage, T., Johnson, S. L., & Raible, D. W. (1999). Nacre encodes a zebrafish microphthalmia-related protein that regulates neural-crest-derived pigment cell fate. *Development*, *126*(17), 3757–3767. https://doi.org/10.1242/dev.126.17.3757
21. McFarland, K. A., Topczewska, J. M., Weidinger, G., Dorsky, R. I., & Appel, B. (2008). Hh and Wnt signaling regulate formation of olig2+ neurons in the zebrafish cerebellum. *Developmental Biology*, *318*(1), 162–171. https://doi.org/10.1016/j.ydbio.2008.03.016
22. Murakami, T., & Morita, Y. (1987). Morphology and distribution of the projection neurons in the cerebellum in a teleost,Sebastiscus marmoratus. *The Journal of Comparative Neurology*, *256*(4), 607–623. https://doi.org/10.1002/cne.902560413
23. Najac, M., McLean, D. L., & Raman, I. M. (2023). Synaptic variance and action potential firing of cerebellar output neurons during motor learning in larval zebrafish. *Current Biology*, *33*(16), 3299-3311.e3. https://doi.org/10.1016/j.cub.2023.06.045
24. Narayanan, S., & Thirumalai, V. (2019). Contributions of the cerebellum for predictive and instructional control of movement. *Current Opinion in Physiology*, *8*, 146–151. https://doi.org/10.1016/j.cophys.2019.01.011
25. Pachitariu, M., Stringer, C., Dipoppa, M., Schröder, S., Rossi, L. F., Dalgleish, H., Carandini, M., & Harris, K. D. (2017). *Suite2p: Beyond 10,000 neurons with standard two-photon microscopy* (p. 061507). bioRxiv. https://doi.org/10.1101/061507
26. Pankratov, Y. V., & Krishtal, O. A. (2003). Distinct Quantal Features of AMPA and NMDA Synaptic Currents in Hippocampal Neurons: Implication of Glutamate Spillover and Receptor Saturation. *Biophysical Journal*, *85*(5), 3375–3387. https://doi.org/10.1016/S0006-3495(03)74757-2
27. Pologruto, T. A., Sabatini, B. L., & Svoboda, K. (2003). ScanImage: Flexible software for operating laser scanning microscopes. *BioMedical Engineering OnLine*, *2*, 13. https://doi.org/10.1186/1475-925X-2-13
28. Proville, R. D., Spolidoro, M., Guyon, N., Dugué, G. P., Selimi, F., Isope, P., Popa, D., & Léna, C. (2014). Cerebellum involvement in cortical sensorimotor circuits for the control of voluntary movements. *Nature Neuroscience*, *17*(9), 1233–1239. https://doi.org/10.1038/nn.3773

29. Remington, S. J. (2011). Green fluorescent protein: A perspective. *Protein Science : A Publication of the Protein Society*, *20*(9), 1509–1519. https://doi.org/10.1002/pro.684
30. Schmahmann, J. D. (2019). The cerebellum and cognition. *Neuroscience Letters*, *688*, 62–75. https://doi.org/10.1016/j.neulet.2018.07.005
31. Sengupta, M., & Thirumalai, V. (2015). AMPA receptor mediated synaptic excitation drives state-dependent bursting in Purkinje neurons of zebrafish larvae. *eLife*, *4*, e09158. https://doi.org/10.7554/eLife.09158
32. Sokolov, A. A., Miall, R. C., & Ivry, R. B. (2017). The Cerebellum: Adaptive Prediction for Movement and Cognition. *Trends in Cognitive Sciences*, *21*(5), 313–332. https://doi.org/10.1016/j.tics.2017.02.005
33. Stein, J. F., & Glickstein, M. (1992). Role of the cerebellum in visual guidance of movement. *Physiological Reviews*, *72*(4), 967–1017. https://doi.org/10.1152/physrev.1992.72.4.967
34. Stringer, C., & Pachitariu, M. (2019). Computational processing of neural recordings from calcium imaging data. *Current Opinion in Neurobiology*, *55*, 22–31. https://doi.org/10.1016/j.conb.2018.11.005
35. Takeuchi, M., Matsuda, K., Yamaguchi, S., Asakawa, K., Miyasaka, N., Lal, P., Yoshihara, Y., Koga, A., Kawakami, K., Shimizu, T., & Hibi, M. (2015). Establishment of Gal4 transgenic zebrafish lines for analysis of development of cerebellar neural circuitry. *Developmental Biology*, *397*(1), 1–17. https://doi.org/10.1016/j.ydbio.2014.09.030
36. Umeda, T., Isa, T., & Nishimura, Y. (2022). Temporal dynamics of the sensorimotor convergence underlying voluntary limb movement. *Proceedings of the National Academy of Sciences*, *119*(48), e2208353119. https://doi.org/10.1073/pnas.2208353119
37. Varma, A., Udupa, S., Sengupta, M., Ghosh, P. K., & Thirumalai, V. (n.d.). A machine-learning tool to identify bistable states from calcium imaging data. *The Journal of Physiology*, *n/a*(n/a). https://doi.org/10.1113/JP284373
38. Zang, Y., & De Schutter, E. (2019). Climbing Fibers Provide Graded Error Signals in Cerebellar Learning. *Frontiers in Systems Neuroscience*, *13*. https://www.frontiersin.org/articles/10.3389/fnsys.2019.00046
39. Zhang, Y., Rózsa, M., Liang, Y., Bushey, D., Wei, Z., Zheng, J., Reep, D., Broussard, G. J., Tsang, A., Tsegaye, G., Narayan, S., Obara, C. J., Lim, J.-X., Patel, R., Zhang, R., Ahrens, M. B., Turner, G. C., Wang, S. S.-H., Korff, W. L., … Looger, L. L. (2023). Fast and sensitive GCaMP calcium indicators for imaging neural populations. *Nature*, *615*(7954), 884–891. https://doi.org/10.1038/s41586-023-05828-9